Journal of Power Sources 196 (2011) 5667–5673

Contents lists available at ScienceDirect

Journal of Power Sources

journal homepage: www.elsevier.com/locate/jpowsour

SiO_x–graphite as negative for high energy Li-ion batteries

A. Guerfi, P. Charest, M. Dontigny, J. Trottier, M. Lagacé, P. Hovington, A. Vijh, K. Zaghib*

Institut de Recherche d'Hydro-Québec, Varennes, QC, Canada J3X 1S1

ARTICLE INFO

Article history:
Received 15 December 2010
Received in revised form 28 January 2011
Accepted 3 February 2011
Available online 12 February 2011

Keywords:
SiO_x
Graphite
Anode
Li-ion batteries
Green transportation

ABSTRACT

Negative electrodes containing SiO_x were investigated as alternative negative electrodes to carbon for Li-ion batteries. The results obtained on the effect of binders and carbon additives on the electrochemical performance (i.e., reversible capacity, coulombic efficiency, charge–discharge rate capability) of the SiO_x–graphite electrode and SiO_x electrode are presented. SEM analysis that utilizes facilities for in situ and ex situ studies were applied to better understand the performance and cycle life of the SiO_x-based electrodes. The SEM analysis clearly showed that the SiO_x particles expand and contract during charge–discharge cycling, and that some of the particles undergo mechanical degradation during this process. The SiO_x–graphite electrode with polyimide binder exhibited a stable capacity of 600 mAh g^{-1} during high-rate charge–discharge from *C*/4 to 1*C*. These results suggest that the use of a flexible binder like polyimide and reasonably small SiO_x particles (nano-particles) facilitates improved cycle life and higher rate capability.

1. Introduction

Carbonaceous materials are typically used in the negative electrode for Li-ion batteries. Because higher energy Li-ion batteries are demanded in electric vehicles, alternative electrode materials are being sought. It has been known for a long time that a metal such as Si [1–3] in the negative electrode provides higher energy in Li-based batteries, but cycle life is problematic, as well as potential safety issues. The volume change that occurs during charge–discharge ultimately leads to mechanical degradation [4–6]. However, when small particles [7,8] or thin-films [9,10] containing silicon are used as the negative electrode, performance and cycle life improve markedly.

Silicon is an attractive alternative material due to its high gravimetric and volumetric capacity density of 4200 mAh g^{-1} and 9800 mAh mL^{-1}, respectively, when the $Li_{4.4}Si$ phase [11–13] is formed. In spite of this advantage, Si-based anodes show numerous problems that prevent the material to be commercial in Li-ion batteries. A significant capacity fade occurs during cycling and low coulombic efficiency is obtained. The performance degrades during the first few cycles due to the large volume change from alloying/de-alloying (charge–discharge) that induces cracks in the micro-size particles and then a failure of electrical contacts. In order to reduce this effect, we have selected the SiO_x mixed with graphite. The characteristic features of SiO_x electrodes are they exhibit less volume change than Si during charge–discharge cycling. In addition, the SiO_x electrodes still have an attractive capacity of 1338 mAh g^{-1}, but they have low first cycle (1st cycle) coulombic efficiency and low electronic conductivity. Takami [28] prepared a nanosilicon cluster comprised of Si, SiO_x and C by disproportionation of silicon monoxide and polymerization of furfuryl alcohol. They reported a reversible capacity of about 1700 mAh g^{-1}. These results are very encouraging, and prompted our effort to investigate SiO_x electrodes for Li-ion batteries."

The aim of this paper is to present the results on the effect of binders and carbon additives on the electrochemical performance (i.e., reversible capacity, coulombic efficiency, charge–discharge rate capability) of the SiO_x–graphite electrode compared to the SiO_x electrode. Yang et al. [14] investigated the electrochemical performance of SiO_x electrodes and obtained promising initial cycle life, but their study only reported results with one binder and with limited charge–discharge rates. Our study extends the earlier study by also presenting results on the morphology changes to the SiO_x particles using in situ and ex situ scanning electron microscopy.

Negative electrodes for Li-ion batteries are mainly composed of carbonaceous materials, but to obtain higher energy density, alternative materials such as metal oxides are receiving considerable attention. As mentioned above, metals such as silicon have high capacity, but mechanical degradation problems encountered during charge–discharge cycling, have led to a closer examination of metal oxide electrodes. In particular, Ti oxide-based electrodes [15–24] have achieved success in Li-ion batteries. The nanocrystalline lithium titanium spinel oxide ($Li_4Ti_5O_{12}$) is a promising negative electrode material because of its excellent rate capability and structural stability, which permits extensive charge–discharge cycling without significant degradation. The major disadvantage

* Corresponding author. Tel.: +1 450 652 8019; fax: +1 450 652 8424.
E-mail address: Zaghib.karim@ireq.ca (K. Zaghib).

0378-7753/$ – see front matter © 2011 Elsevier B.V. All rights reserved.
doi:10.1016/j.jpowsour.2011.02.018

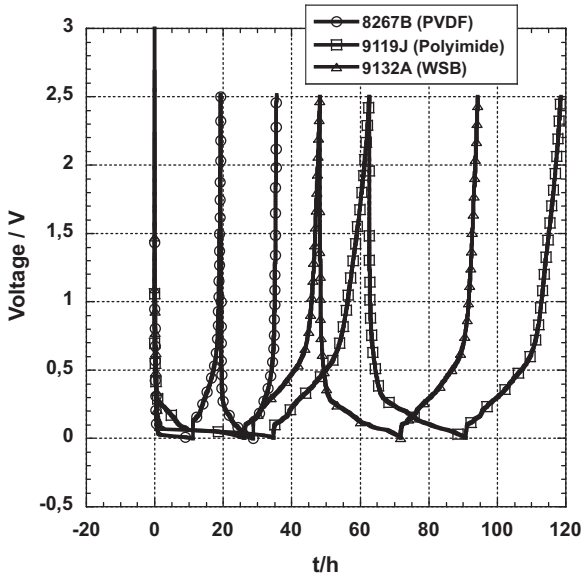

Fig. 1. Charge–discharge cycling of SiO_x–graphite electrodes containing PVDF, WSB or polyimide binder. *C*/25 rate was used.

Table 1
Coulombic efficiency and capacities for charge and discharge of cells with different binders.

Binder	Cycle 1	Cycle 2
PVDF		
Charge (mAh g^{-1})	642	541
Disc (mAh g^{-1})	472	394
EC (%)	74	73
WDB		
Charge (mAh g^{-1})	919	778
Disc (mAh g^{-1})	817	778
EC (%)	85	95
Polyimide		
Charge (mAh g^{-1})	1283	1024
Disc (mAh g^{-1})	1026	1026
EC (%)	80	99

of $Li_4Ti_5O_{12}$ for high-energy Li-ion batteries is its high Li^+ insertion potential, about 1.5 V *vs.* Li/Li^+. Despite our success with $Li_4Ti_5O_{12}$ electrodes, we expanded our investigated to SiO_x electrodes because of their higher capacity and larger operating voltage range, closer to 0 V *vs.* Li/Li^+ upon discharge, compared to about 1.5 V for $Li_4Ti_5O_{12}$.

The binder has an important effect on the performance of the anode and the interface between the anode particles. The binder

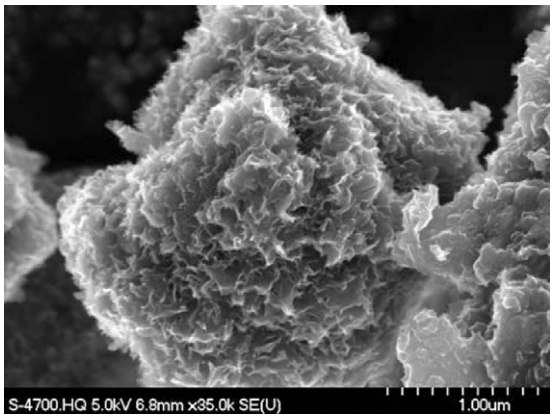

Fig. 2. SEM of SiO_x–graphite.

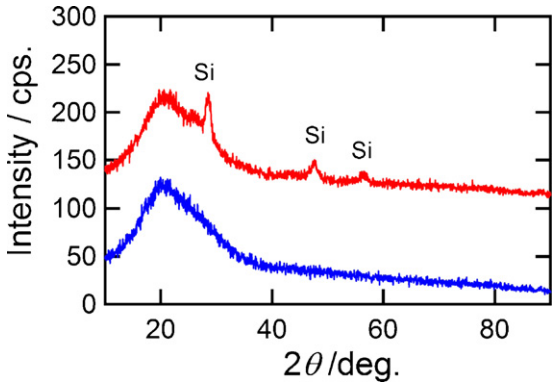

Fig. 3. XRD of pure SiO_x (blue curve) and carbon-coated SiO_x (red curve). (For interpretation of the references to color in this figure legend, the reader is referred to the web version of the article.)

also plays a significant role in electrode performance because it forms a solid–electrolyte interface (SEI) film, which depends on the binder composition. By using a variety of binders having different chemical and mechanical properties, different performance of the SiO_x anode will be obtained. To further improve our comprehension on the SEI layer with SiO_x and its mixture with graphite, two analysis methods will be used: ex situ SEM on cycled anodes with standard electrolyte, and in situ SEM during anode cycling. We plan to use an ex situ SEM analysis for some binders, but the in situ experiments will use dry polymer binder in the anode to avoid the issue with electrolyte evaporation.

2. Experimental

2.1. Materials

Three types of binders were used in this study; poly(vinylidene fluoride) (PVDF) from Kruha, Japan, CMC-based water dispersed binder (WDB) from Zeon Japan and polyimide (Aldrich). The SiO_x ($x \sim 0.95$), which was obtained from ShinEtsu (Japan), has an 7-μm average particle size. To enhance the conductivity, the SiO_x particles were coated with a thin layer of carbon (~1 nm thickness). The exact amount of oxygen in the sample was determined by a Leco-TC400.

The natural graphite (OMAC1S, 15-μm average particle size) was obtained from Osaka Gas (Japan). The electrodes were prepared by mixing SiO_x and graphite (1:1 weight ratio) with the binder dissolved in *N*-methyl-2-pyrrolidinone (NMP) for PVDF and polyimide, and in water for WDB, in the weight ratio 10%, 15% and 5%, respectively. A small fraction of vapor-grown carbon fibers (2% VGCF from Showa-Denko, Japan) was added to each of the electrode compositions. The slurries are coated on copper foil and dried at 120 °C for the PVDF and WDB and higher at 150 °C for the polyimide [30] for 24 h under vacuum, and then compressed. The cells were assembled in an argon-filled glove box.

2.2. Electrochemical tests

The charge–discharge measurements were carried out in CR2025 coin-type cells with a lithium metal counter electrode, Celgard 3501 separator and electrolyte of 1 M $LiPF_6$ in a mixture of ethylene carbonate (EC) and diethyl carbonate (DEC) at ambient temperature (25 °C). In some experiments, 2% vinyl carbonate (VC) was added to the electrolyte. In these experiments, discharge refers to a mechanism involving the insertion of Li^+ ions in SiO_x as the cell voltage decreases to close to 0 V. Charge refers to a change in the cell voltage from about 0 V to about 2.5 V where Li^+ ions leaves the SiO_x

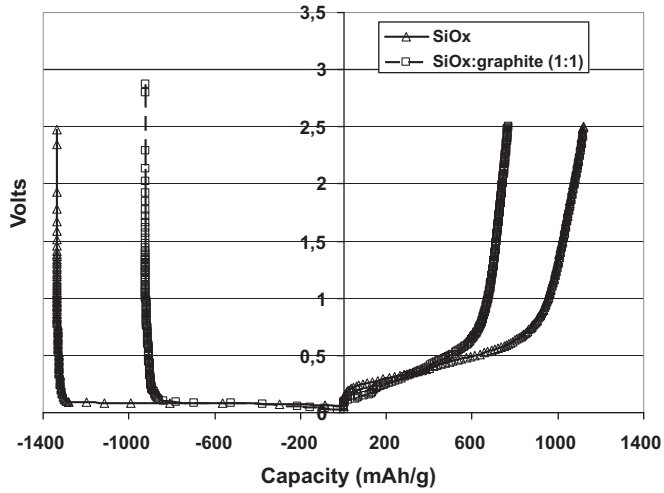

Fig. 4. Charge–discharge potential profile for SiO_x and SiO_x–graphite electrodes at $C/24$ rate. Electrolyte is 1 M $LiPF_6$–EC–DEC and binder is WDB. Discharge is left panel and charge is right panel.

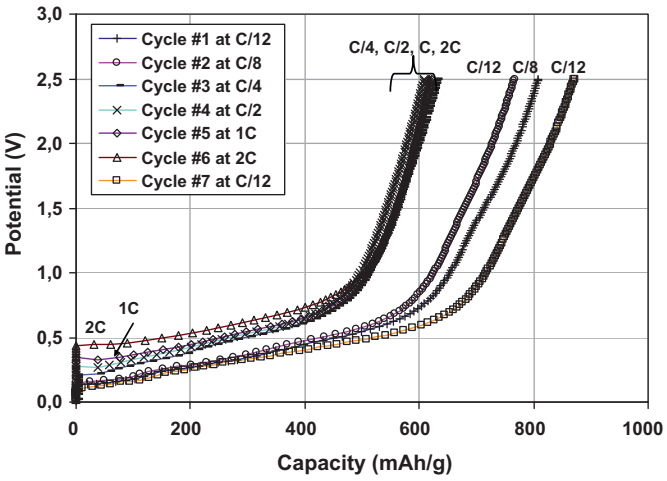

Fig. 5. Effect of charge–discharge rate ($C/12$–$1C$ rate) on SiO_x–graphite electrodes. Electrolyte is 1 M $LiPF_6$–EC–DEC + 2% VC and binder is polyimide.

structure. The tests were evaluated with a multi-channel battery cycler (Macpile®, Claix, France).

2.3. Materials characterization

The electrodes containing SiO_x were examined by in situ SEM (scanning electron microscopy) using a SEM 2400 (Hitachi, Japan). The in situ SEM observations can be made with a plane (top) view or in cross-section view of the electrode. Additional details on electrode preparation and operational procedures of the SEM are described elsewhere by Zaghib et al. [25–27]. Because of solvent evaporation in the vacuum in the SEM chamber, a dry solid polymer binder was used in the electrodes. The intent of these experiments is to better understand the cycling behaviour of SiO_x and the failure mode associated with capacity fade on cycling and at higher rates.

3. Results and discussion

The results obtained from electrochemical measurements and SEM observations of SiO_x and SiO_x–graphite electrodes are presented. A major objective of this study is to determine the viability

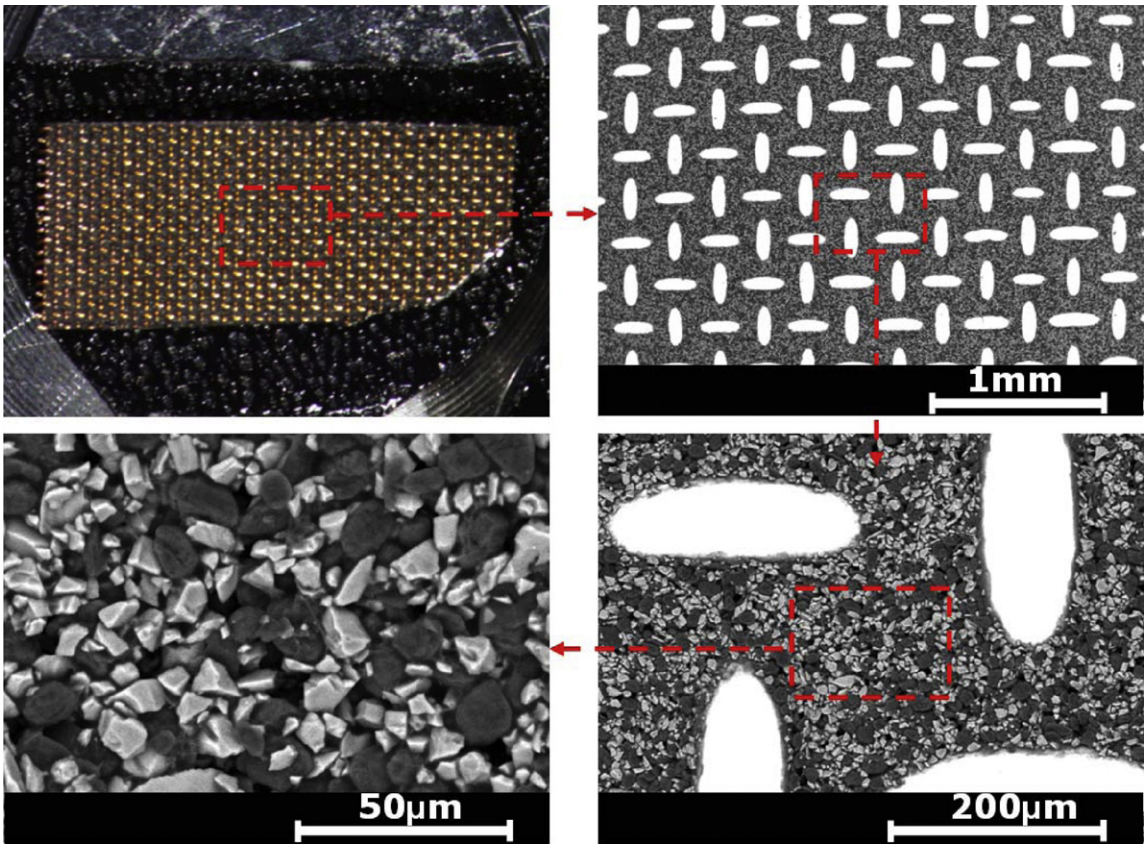

Fig. 6. SEM micrograph of SiO_x–graphite electrodes on exmet.

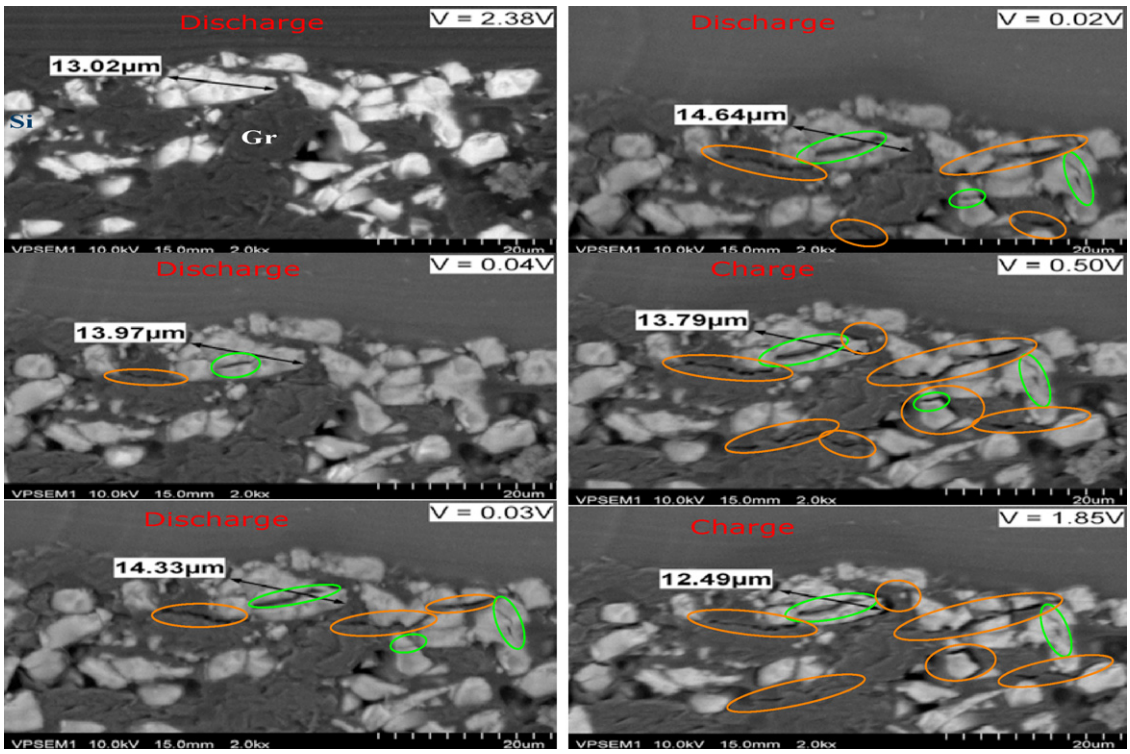

Fig. 7. In situ SEM images of cross-section of SiO_x–graphite electrode at different potentials during charge–discharge cycling.

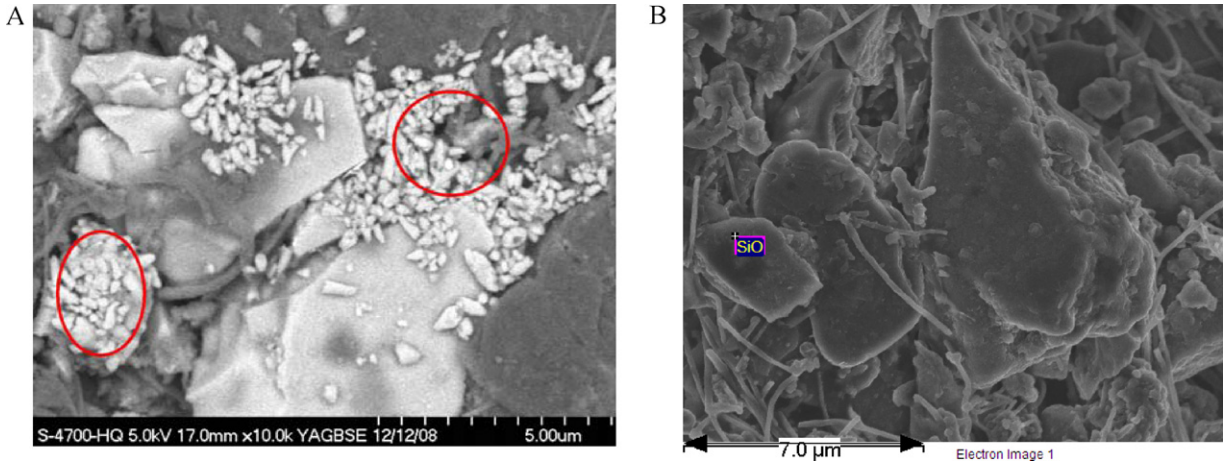

Fig. 8. Ex situ SEM analysis of SiO_x particles that were cycled at *C*/24 rate. (A) Before cycling and (B) discharge 0.5 V.

of an alternative electrode material, namely SiO_x, for the negative electrode in Li-ion batteries.

3.1. Effect of binder

The effect of the binder on the charge–discharge cycling performance of SiO_x–graphite electrodes was evaluated in 1 M $LiPF_6$–EC–DEC + 2% VC. Fig. 1 shows the different initial cycling response of the electrodes containing PVDF, WSB or polyimide. The charge–discharge cycling of cells containing the different binders were evaluated between cell voltage limits of 2.5 V and 5 mV. Table 1 summarizes the performance of the SiO_x–graphite electrodes for the first two cycles at *C*/24 rate (full charge in 24 h). The highest reversible capacity was found with cells containing polyimide binder, followed by WDB and then PVDF. The cell with WDB had the highest 1st cycle coulombic efficiency (CE), followed by polyimide and then PVDF. However, the CE for the second cycle cells with the polyimide binder was the highest. In addition the cells with the polyimide binder exhibited the highest charge and discharge capacities.

These results show that the binder has an important influence on the performance of the electrode and the interface between the SiO_x particles. The binder also plays a significant role in electrode performance because it affects the formation of the SEI layer. By using a variety of binders having different chemical and mechanical properties, different performance of the SiO_x was obtained. The polyimide and WDB binders do not contain fluorine, which may be beneficial when LiF is formed to stabilize the SEI layer. The results of EDX (not presented here) clearly showed the presence of fluoride ions in the SEI layer during potential decrease to <0.8 V. The SEI passivation layer on graphite and SiO_x is different. Because the

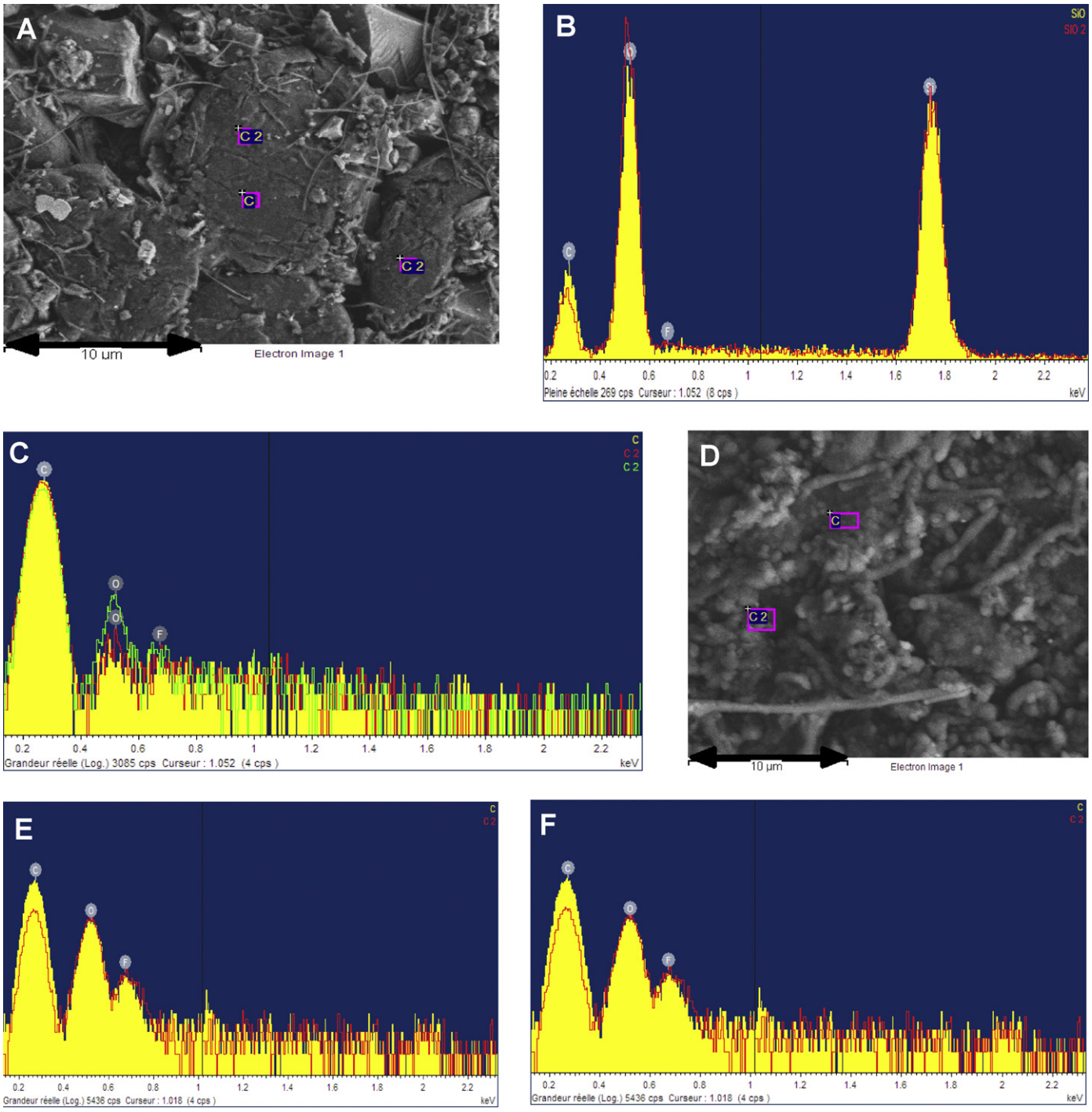

Fig. 9. Ex situ SEM and EDX of SEI layer on graphite and SiO_x at different voltages: (A) discharge at 0.2 V, (B) EDX at 0.2 V, (C) EDX at 0.2 V, (D) discharge at 0 V, (E) EDX at 0 V, and (F) EDX at 0 V.

volume change during charge–discharge on SiO_x is much greater than that on graphite, the SEI layer suffers mechanical breaks and an interface that is not homogenous is formed. Thus, the presence of graphite in the SiO_x–graphite electrode helps to form a more stable SEI layer.

To further improve our comprehension on the SEI layer with SiO_x and its mixture with graphite, two analysis methods were used; ex situ SEM on cycled electrodes with standard electrolyte and in situ SEM to observe changes taking place during electrode cycling. These results are discussed later in the paper.

3.2. Morphology of SiO_x–graphite

The morphology of the SiO_x–graphite particles was examined by SEM. Fig. 2 shows that the surface of the SiO_x particles is covered with platlet-like carbon. Because the carbon in the electrode composition is graphite, the small graphite layers coat the SiO_x particles. In Fig. 3, the XRD of pure SiO_x is illustrated by the blue curve and the red curve is the XRD pattern of carbon-coated SiO_x. The XRD pattern of carbon-coated SiO_x shows evidence for the presence of Si but no carbon because the coating is too thin (1 nm) to detect by X-rays. Close examination by TEM showed that nano-domains of Si were

present in the SiO/SiO_2 matrix. The presence of Si in the carbon-coated SiO_x may be due to the reaction of Si oxide and C, which reduces the oxide to metallic Si during preparation. However, no systematic study was undertaken to verify this explanation.

3.3. Comparison of charge–discharge of SiO_x and SiO_x–graphite

A comparison of the charge–discharge potential curves at *C*/24 for SiO_x and SiO_x–graphite electrodes is shown in Fig. 4. The reversible capacity of the electrode with only SiO_x (1338 mAh g^{-1}) is higher than that of SiO_x–graphite (980 mAh g^{-1}), but the coulombic efficiency of the two electrodes is comparable (about 84%). The presence of graphite decreases the capacity and increases the conductivity of the electrode. The capacity of the SiO_x–graphite also accounts for the weight of graphite, consequently a lower capacity is expected. The irreversible capacity loss is due the formation of the SEI layer on SiO_x and graphite surfaces, and the formation Li_2O, were evident from by EDX and SEM analysis.

3.4. Rate capability

The effect of charge rate (*C*/12 (12 h)–2*C* (2 h) rate) was investigated with SiO_x–graphite electrodes that were fabricated with polyimide binder (see Fig. 5). In these studies, the discharge rate is constant at *C*/12. These experiments were conducted with the electrolyte 1 M $LiPF_6$–EC–DEC + 2% VC. A stable capacity of about 600 mAh g^{-1} was observed at rates from *C*/4 to 1*C* (cycle #3–6), and the cell was still able to deliver a capacity of >800 mAh g^{-1} at *C*/12 rate during cycle #7 to a cut-off voltage of 2.5 V. These results suggest that the SiO_x–graphite electrode was not adversely affected by the high charge–discharge rate up to 1*C*, at least in these preliminary studies.

3.5. In situ and ex situ SEM analysis

SEM analysis that utilizes facilities for in situ and ex situ studies were applied to better understand the performance and cycle life of the SiO_x-based electrodes. The sequence of micrographs at progressively increasing magnification in Fig. 6 shows SiO_x–graphite on copper exmet screen. The geometric pattern of the exmet screen is clearly evident in the micrographs. At the highest magnification (lower right-hand corner), the carbon-coated SiO_x and graphite particles are clearly distinguished by the lighter and darker colors, respectively. The carbon-coated SiO_x is mixed with graphite particles, which produced the distinctly different shades in the SEM micrograph.

A post-mortem analysis of SiO_x–graphite electrodes was conducted by in situ SEM. The in situ SEM analysis of the electrode surface, observed through the collector mesh holes, showed no observable changes had occurred. However, in situ SEM of the electrode cross-section showed the effects of expansion/contraction of the SiO_x particles during charge and discharge. The result (see Fig. 7) revealed that the bigger particles (~13 μm) start to exhibit cracks at around 0.1 V during discharge. Some fissures were observed and the particles become delaminated. The fissures showed a larger volume change when the electrode is discharged deeply. When the potential during discharge reaches 0.03 V, the 13.02-μm particle has expanded to 14.64 μm. The power of the in situ SEM analysis is evident in that changes in the morphology of a single particle can be observed during charge–discharge cycling, in real time. During the charging process, all the cracks remained; some fissures collapsed and others swelled. The dimensions of the SiO_x particles that expanded (for example, 14.64 μm) during discharge, diminished in size upon charge to 1.85 V. Video 1 of the top of the electrode show no change of the volume of the particle, however Video 2 for the cross-section show the volumetric expansion related to Fig. 7. In general, it appears that the smaller particles (<2 μm) did not crack because these particles have higher surface area, and the SEI layer is more stable due to the low volumetric expansion. From this result, it suggests that smaller particles combined with more elastic binder are better for achieving long cycle life without mechanical degradation of the SiO_x particles. These studies will help to better understand the cycling mechanism of SiO_x and the failure mode associated with capacity fade.

Ex situ SEM was used to observe the SiO_x particles before and after cycling at *C*/24 rate. The micrograph in Fig. 8 shows the initial SiO_x particles are relatively large before cycling. However, after cycling, some of the initial particles disintegrated to form numerous smaller SiO_x particles (areas highlighted by circular red lines), which are more prevalent after discharge to 0.5 V during the first cycle. These observations illustrate that the expansion and contraction of the SiO_x particles leads to mechanical degradation and the formation of much smaller particles. The analysis of the SEI layer at different voltages is described in Fig. 9. Some O and F were found at different locations on the surface of graphite at 0.250 V, before lithium intercalated tin the graphite. Strong peaks for O and F were observed, confirming a thicker SEI layer for both C and SiO_x was present. The C peak was detected at the SiO_x surface (0.0 V) when the graphite is fully intercalated (LiC_6). Local chemical mapping (at discharged state at 0 V) shows that the F was non-uniformly dispersed, in particular on the surface of SiO_x. The SEI layer is stable on the graphite surface [29].

4. Conclusion

The electrochemical performance of SiO_x as an alternative to graphite for the negative electrode was investigated in cells containing a Li counter electrode. The influence of the binder (e.g., polyimide, WSB, PVDF) on charge–discharge capacity and coulombic efficiency was determined. The highest reversible capacity of the SiO_x–graphite electrode was observed with the polyimide binder, and the lowest capacity was obtained in a cell containing PVDF binder. The cell with the polyimide binder also had the highest coulombic efficiency after the second cycle.

The SiO_x–graphite electrode with polyimide binder exhibited a stable capacity of 600 mAh g^{-1} during high-rate charge–discharge from *C*/4 to 1*C*. These results suggest that the use of a flexible binder like polyimide and reasonably small SiO_x particles facilitates improved cycle life and higher rate capability.

The power of in situ SEM for observing morphological changes to the SiO_x particles was demonstrated. The findings from the in situ SEM observations suggest that smaller SiO_x particles (nano-particles) and more flexible binders are necessary to obtain electrodes with improved charge–discharge cycling performance. The graphite addition improves the rate capability and cyclability of the anode due to its high conductivity and having more stable SEI compared to SiO_x particles.

Acknowledgements

The authors would like to thank the DOE-BATT program and Hydro-Québec for support of this work.

Appendix A. Supplementary data

Supplementary data associated with this article can be found, in the online version, at doi:10.1016/j.jpowsour.2011.02.018.

References

[1] T. Takamura, S. Ohara, M. Uehara, J. Suzuki, K. Sekine, J. Power Sources 129 (2004) 96.
[2] X. Yang, Z. Wen, X. Xu, B. Lin, Z. Lin, J. Electrochem. Soc. 153 (2006) A1351.
[3] D. Larcher, S. Beattie, M. Morcrette, K. Edstrom, J.-C. Jumas, J.-M. Tarascon, J. Mater. Chem. (2007), doi:10.1039/b705421c.
[4] J.H. Ryu, J.W. Kim, Y.-E. Sung, S.M. Oh, Electrochem. Solid State Lett. 7 (2004) A306.
[5] M.N. Obrovacz, L. Christensen, Electrochem. Solid State Lett. 7 (2004) A93.
[6] M. Yoshio, T. Tsumura, N. Dimov, J. Power Sources 146 (2005) 10.
[7] J. Graetz, C.C. Ahn, R. Yazami, B. Fultz, Electrochem. Solid State Lett. 6 (2003) A194.
[8] X.-W. Zhang, P.K. Patil, C. Wang, A. John Appleby, F.E. Little, D.L. Cocke, J. Power Sources 125 (2004) 206.
[9] K.-L. Lee, J.-Y. Jung, S.-W. Lee, H.-S. Moon, J.-W. Park, J. Power Sources 129 (2004) 230.
[10] J.P. Maranchi, A.F. Hepp, P.N. Kumta, Electrochem. Solid State Lett. 6 (2003) A198.
[11] M.N. Obrovac, L. Christensen, D.B. Le, J.R. Dahn, J. Electrochem. Soc. 154 (2007) A849.
[12] Y. Kobayashi, S. Seki, Y. Ohno, H. Miyashiro, P. Charest, A. Guerfi, K. Zaghib, J. Power Sources 185 (2008) 542.
[13] H.S. Kim, K.Y. Chung, B.W. Cho, J. Power Sources 189 (2009) 108.
[14] J. Yang, Y. Takeda, N. Imanishi, C. Capiglia, J.Y. Xie, O. Yamamoto, Solid State Ionics 152-153 (2002) 125.
[15] A. Guerfi, S. Sévigny, M. Lagacé, P. Hovington, K. Kinoshita, K. Zaghib, J. Power Sources 119–121 (2003) 88.
[16] A. Guerfi, P. Charest, K. Kinoshita, M. Perrier, K. Zaghib, J. Power Sources 126 (2004) 163.
[17] K. Zaghib, M. Simoneau, M. Armand, M. Gauthier, J. Power Sources 81–82 (1999) 300.
[18] C. Jiang, Y. Zhou, I. Honma, T. Kudo, H. Zhou, J. Power Sources 166 (2007) 514.
[19] C.-L. Wang, Y.C. Liao, F.C. Hsu, N.H. Tai, M.K. Wu, J. Electrochem. Soc. 152 (2005) A653.
[20] J. Li, Z. Tang, Z. Zhang, Electrochem. Solid State Lett. 8 (2005) A316.
[21] C. Bohnke, J.-L. Fourquet, N. Randrianantoandro, T. Brousse, O. Crosnier, J. Solid State Electrochem. 6 (2002) 403.
[22] J. Gao, C. Jiang, J. Ying, C. Wan, J. Power Sources 155 (2006) 364.
[23] M. Venkateswarlu, C.H. Chen, J.S. Do, C.W. Lin, T.C. Chou, B.J. Hwan, J. Power Sources 146 (2005) 204.
[24] M. Kalba, M. Zukalova, L. Kavan, J. Solid State Electrochem. 8 (2003) 2.
[25] K. Zaghib, P. Hovington, M. Lagacé, A. Guerfi, P. Charest, in: K. Zaghib, C.M. Julien, J. Prakash (Eds.), ECS Proceeding Volume PV 2003-20, New Trends in Intercalation Compounds for Energy Storage and Conversion, The Electrochemical Society, Pennington, NJ, 2003, p. 670.
[26] K. Zaghib, M. Armand, M. Gauthier, J. Electrochem. Soc. 145 (1998) 3135.
[27] K. Zaghib, M. Armand, M. Gauthier, in: J. Broadhead, B. Scrosati (Eds.), Proceedings of the Symposium on Lithium Polymer Batteries, The Electrochemical Society, Pennington, NJ, 1997, p. 250.
[28] T. Morita, N. Takami, J. Electrochem. Soc. 153A (2006) 425.
[29] C. Doh, C. Park, H. Shin, D. Kim, Y. Chung, S. Moon, B. Kim, A. Veluchamy, J. Power Sources 179 (2008) 367.
[30] Y. Kobayashi, S. Seki, Y. Mita, Y. Ohno, H. Miyashiro, P. Charest, A. Guerfi, K. Zaghib, J. Power Sources 185 (2008) 542.